

Hierarchical Slice Patterns Inhibit Crack Propagation in Brittle Sheets


Michael Zaiser,¹ Seyyed Ahmad Hosseini¹,^{1b} Paolo Moretti,¹ Tero Mäkinen^{1b},^{2,3,*} Juha Koivisto,² Mahshid Pournajar,¹ Marcus Himmler,⁴ Michael Redel,⁴ Dirk W. Schubert,⁴ and Mikko J. Alava^{2,3}

¹*Institute of Materials Simulation, Department of Materials Science, Friedrich-Alexander University Erlangen-Nürnberg, Dr. Mack Strasse 77, Fürth 90762, Germany*

²*Department of Applied Physics, Aalto University, P.O. Box 11000, Aalto, Espoo 00076, Finland*

³*NOMATEN Centre of Excellence, National Centre for Nuclear Research, ul. A. Soltana 7, Otwock-Świerk 05-400, Poland*

⁴*Institute of Polymer Materials, Department of Materials Science, Friedrich-Alexander University Erlangen-Nürnberg, Martensstr. 7, Erlangen 91058, Germany*

 (Received 7 April 2022; revised 25 April 2022; accepted 8 September 2022; published 14 October 2022)

By introducing hierarchical patterns of load-parallel cuts into axially loaded brittle sheets, the resistance to propagation of mode-I cracks is very significantly enhanced. We demonstrate this effect by simulation of two-dimensional beam network models and experimentally by testing paper and polystyrene (PS) sheets that are sliced with a laser cutter to induce load-perpendicular hierarchical cut patterns. Samples endowed with nonhierarchical reference patterns of the same cut density and nonsliced sheets are considered for comparison. We demonstrate that hierarchical slicing can increase failure load, apparent fracture toughness, and work of fracture of notched paper and PS sheets by factors between 2 and 10.

DOI: [10.1103/PhysRevApplied.18.044035](https://doi.org/10.1103/PhysRevApplied.18.044035)

I. INTRODUCTION

Materials with hierarchical microstructures consist of microstructural elements, which have themselves internal structure, forming patterns where similar (micro)structural features are reproduced on multiple scales in a self-similar manner. Such hierarchical microstructures are encountered in past, present, and future technological systems—an often cited real-world example being the three-level iron girder skeleton of the Eiffel tower [1], a much more speculative one being the five-level self-similar space elevator cable made of carbon nanotubes that was suggested in Ref. [2]. In particular, hierarchical microstructures are ubiquitous in biomaterials [3]. An example is the hierarchical modular organization of collagen, ranging from molecules over microfibrils and fibers to hierarchical fiber bundles, ensuring enhanced toughness of the hierarchical structure over that of an assembly of isolated collagen molecules [4]. Other examples include the hierarchical structure of bone [5,6], the cellular structure of wood [3], or the hierarchical lamellar microstructure of tortoise shells [7].

Fracture mechanics of hierarchical materials was studied in a series of papers by Gao and co-workers [8,9]. In these works it was demonstrated that hierarchical microstructure can be considered as a method to achieve

damage tolerance, i.e., to mitigate against catastrophic propagation of a localized flaw driven by stress concentrations. The basic idea is that if we envisage fracture within the framework of cohesive crack models, then the crack tip is always preceded by a fracture process zone, the extension of which depends on the elastic properties of the material and the shape of the cohesive law. If the extension of the process zone is larger than the characteristic dimension of the remaining intact cross section of the material, then failure no longer occurs by crack propagation but by homogeneous overloading of the intact part. This well-known fact means that, in homogeneous materials, error tolerance can be found only in small-scale samples. The key point is now that in hierarchical materials, as we make a transition to a higher hierarchical level, the cohesive zone may increase in proportion, such that ideally error tolerance can be achieved on all scales. In the work of Gao *et al.* [8,9], this aspect was investigated for two-phase composites where hard platelets are embedded, in a self-similar manner, into a soft matrix. In the present study we take the concept of flaw tolerance by structural hierarchy one step further: we demonstrate that it is possible to achieve flaw tolerance even in single-phase materials, by redesigning the patterns of stress transmission through an educated process of material *removal*.

Similar concepts have been studied in kirigami materials, which are superelastic sheet materials that have a very large degree of tunability of mechanical response

*Corresponding author. tero.j.makinen@aalto.fi

[10,11]. They can be used in wide variety of applications, e.g., medical [12] and electrical applications [13,14] as well as other nanoscale materials [15]. Machine-learning approaches [16,17] have also been used in optimizing their structure. However, the basic deformation mechanisms of these materials are different from that in our approach. Kirigami materials exhibit nonlinear elasticity [18–20] through opening of the gaps in the material by stretching and bending of the structure.

Lattice models are a common tool for studying the failure behavior of quasibrittle materials with microstructural disorder (hence, fluctuating local strength), for an overview see Ref. [21]. In particular, the failure behavior of lattices endowed with a self-similar structural hierarchy was investigated for two-dimensional (2D) fuse lattices [22] and beam lattices [23], and compared with the behavior of nonhierarchical reference structures. The investigations demonstrated the existence of two different failure modes: while non hierarchical structures fail by nucleation and subsequent propagation of a critical crack, hierarchical structures fail by diffuse damage nucleation and coalescence. While these investigations considered the behavior of structures without pre-existing cracks, it may be conjectured that hierarchical structures of the same type might efficiently mitigate against the effect of crack-tip stress concentrations even when large macroscopic cracks are present. Here we directly test this hypothesis, first by simulations of hierarchically structured 2D beam networks containing pre-existing cracks of varying length and then by experiments on quasi-two-dimensional materials, testing notched sheets of paper and polystyrene (PS) endowed with comparable hierarchical patterns.

II. RESULTS

A. Simulations

Simulations are carried out on 2D hierarchical beam networks with deterministic (DHBN) and stochastic (SHBN) morphology. Nonhierarchical reference structures including fully connected networks (FBN) and networks with random gap patterns (RBN) are simulated for comparison. The method of network construction is detailed in Appendix A, and Figs. 1(a) and 1(b) give illustrative examples of DHBN, SHBN, and RBN structures. The simulated networks contain pre-existing cracks of varying length $0 \leq a < L$ where L is the network cross section. In the case of hierarchical structures, the location of the cracks is shifted randomly relative to the hierarchical pattern, however, in all cases the “gaps” of the pattern are oriented perpendicular to the initial crack.

The samples are loaded in tension by imposing, in the crack-perpendicular direction, a global displacement that is monotonically increased until failure occurs. Details of the testing protocol are provided in Appendix A.

Failure of cracked nonhierarchical structures [Fig. 2(a), left and Movie S1 within the Supplemental Material [24]] is found to follow a classical fracture mechanics scenario: upon loading, stress concentrations develop at the crack tips until the crack becomes critical, and failure then proceeds by crack propagation, which is sustained by the release of elastic energy stored in the sample. In hierarchical structures [Fig. 2(a), right and Movie S1 within the Supplemental Material [24]], on the other hand, crack-tip stress concentrations are absent and failure therefore requires a much higher overall stress level. Even then, the existing crack either does not propagate at all or is rapidly arrested, whence failure proceeds by nucleation and subsequent arrest of new cracks nucleated at other locations in the sample. As a consequence, both peak stresses and post-peak activity in hierarchical samples significantly exceed those in the nonhierarchical reference structures, as seen on the stress-strain curves in Fig. 2(b). The differences are also reflected in the crack length dependence of the peak stress supported by the samples. Here the findings on nonhierarchical structures closely follow the predictions of quasibrittle fracture mechanics. Thus, the peak load σ_p supported by a sample decreases in approximately inverse proportion with the square root of crack length,

$$\sigma_p = \frac{K_{Ic}}{\sqrt{\pi(a + a_0)}} f\left(\frac{a}{L}\right), \quad (1)$$

where a_0 is a process zone size [25] and the function $f(a/L)$ accounts for specimen size effects, see red data points and red line in Fig. 2(c); the red line has been calculated from Eq. (1) with $f(x) = (x/\tan x)^{1/2}$, $x = \pi a/(2L)$ as appropriate for a L -periodic array of cracks loaded in parallel [26]. Equation (1) characterizes the size effect of classical fracture mechanics, where strength decreases approximately in inverse proportion with the square root of crack length. In hierarchical samples, on the other hand, we observe a linear decrease of the supported load, which is simply proportional to the intact sample cross section,

$$\sigma_p = \sigma_p(a=0) \left(1 - \frac{a}{L}\right). \quad (2)$$

This is the behavior expected for a bundle of parallel unconnected fibers: if a “crack” cuts a fraction a/L of the fibers, then the load that can be carried by the structure decreases by a factor $(1 - a/L)$. However, bundles of unconnected fibers are not a good solution for a load-carrying structure [27] since they are prone to a different type of size effect, which is of statistical origin, as the unconnected fibers fail at their respective weakest cross sections. This may lead to a very significant reduction of overall strength, which is absent in our hierarchical structures, as discussed in Appendix C.

Thus, hierarchical samples mitigate both against fracture mechanical and statistical size effects. As a consequence,

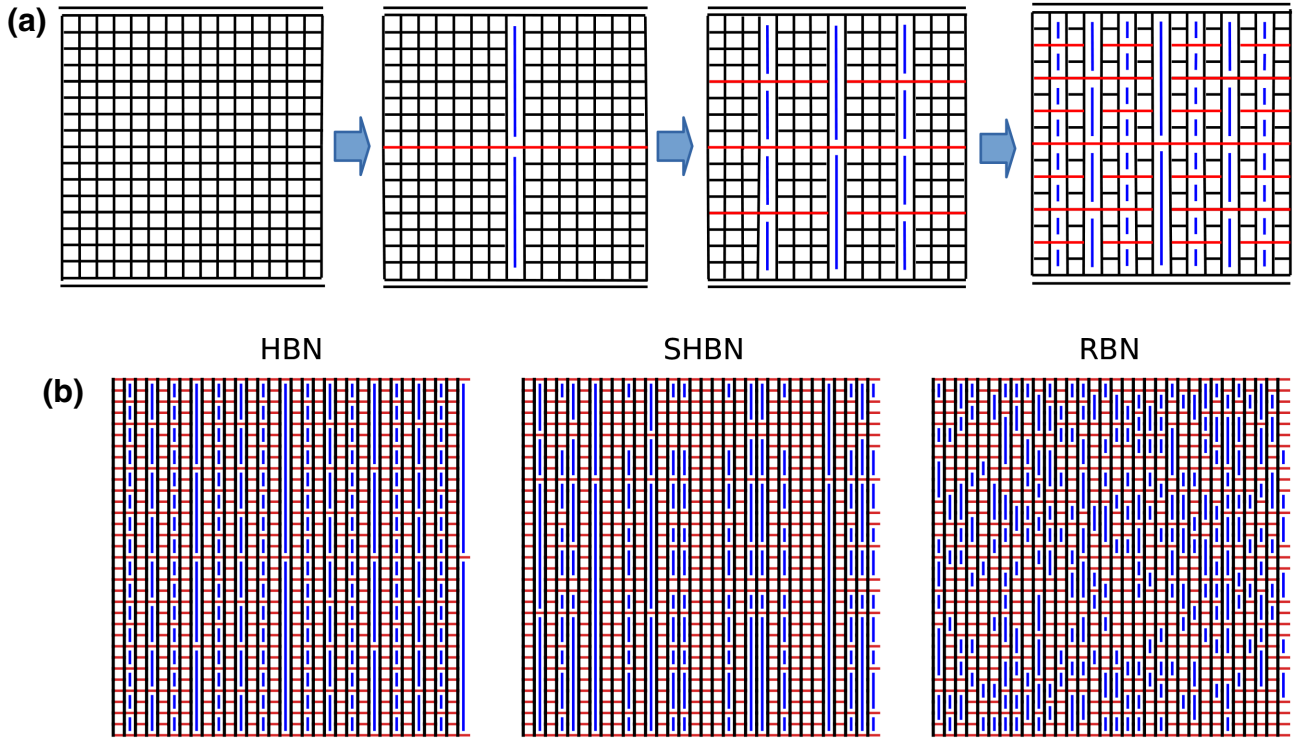


FIG. 1. Hierarchical patterning. (a) “Top-down construction” of a $n = 4$ -level-HBN structure: we start with a solid plate represented by a 2D FBN of size L ; this is then divided by two load-parallel cuts into four lower-level modules—two groups of two modules loaded in series, connected by a remaining, system spanning cross-link (CL) connector of length L ; then each of the four modules is again divided by two shorter cuts into four lower-level modules plus a module-spanning CL connector of length $L/2$, etc.; cuts are marked in blue, the remaining CL connectors are colored red. (b) Five-level HBN structure together with randomly permuted SHBN structure and reference RBN structure, illustrating the patterns of cuts and connectors for the different structures.

the load supported by hierarchical samples may very significantly exceed that of their nonhierarchical counterparts [blue data points and blue line in Fig. 2(c)]. The same is true for the specific work of fracture (WOF) $w_F = W_F/[t(L - a)]$, defined as the mechanical work $W_F = V \int \sigma(\epsilon) d\epsilon$ needed to fully break the sample from its initial configuration (V is the sample volume), divided by the initial area $t(L - a)$ of the intact ligament where t is the sheet thickness [Fig. 2(d)]: after an initial transient, the specific WOF is independent of crack length for both hierarchical and nonhierarchical samples, but for hierarchical samples, the saturation level is about a factor of 5 higher.

To interpret this observation in more detail, we note that the WOF $w_F = w_{F,e} + w_{F,ne}$ can be envisaged as a sum of the work $w_{F,e}$ needed to create the fracture surface, e.g., by propagating a crack across the sample (so-called essential work of fracture [28]) and the work $w_{F,ne}$ dissipated by plastic deformation or damage in the bulk of the sample away from the fracture surface (nonessential work of fracture). In the case of failure by crack propagation, the essential work of fracture equals the critical J integral, $w_{F,e} = J_c$ [29], and for an elastic-brittle material failing by crack propagation, $w_{F,e} = J_c = G_c$ equals

the critical energy release rate. For such a material we can thus directly relate the fracture toughness and the essential work of fracture via $K_{Ic}^2 = EG_c = Ew_{F,e}$ where E is, in case of plane-stress deformation as considered here, equal to Young’s modulus of the material. Moreover, for such a material a plot of the WOF versus crack length reaches, after an initial transient related to the process zone size a_0 , a plateau where the WOF is independent on crack length a . This plateau value can then directly be related to the essential WOF required for propagating the crack.

We illustrate this for the data from our simulations of samples with precracked RBN patterns, which are well described by Eq. (1). In this case, the fit of Eq. (1) to the data [red line in Fig. 2(c)] yields a fracture toughness $K_{Ic} = 0.0594 \langle \sigma_B \rangle \sqrt{L}$. Assuming brittle crack propagation, this corresponds to an essential work of fracture $w_{F,e} = K_{Ic}^2/E = 0.0035 \langle \sigma_B \rangle^2 L/E$. We can compare this with the plateau value of the specific work of fracture, which from Fig. 2(d) is found to be $w_F \approx 0.047 \langle \sigma_B \rangle^2 L/E$. The comparison shows that in the plateau region, most of the work of fracture in RBN structures corresponds to the essential WOF needed for brittle propagation of the pre-existing crack. For the hierarchical structures, on the other hand,

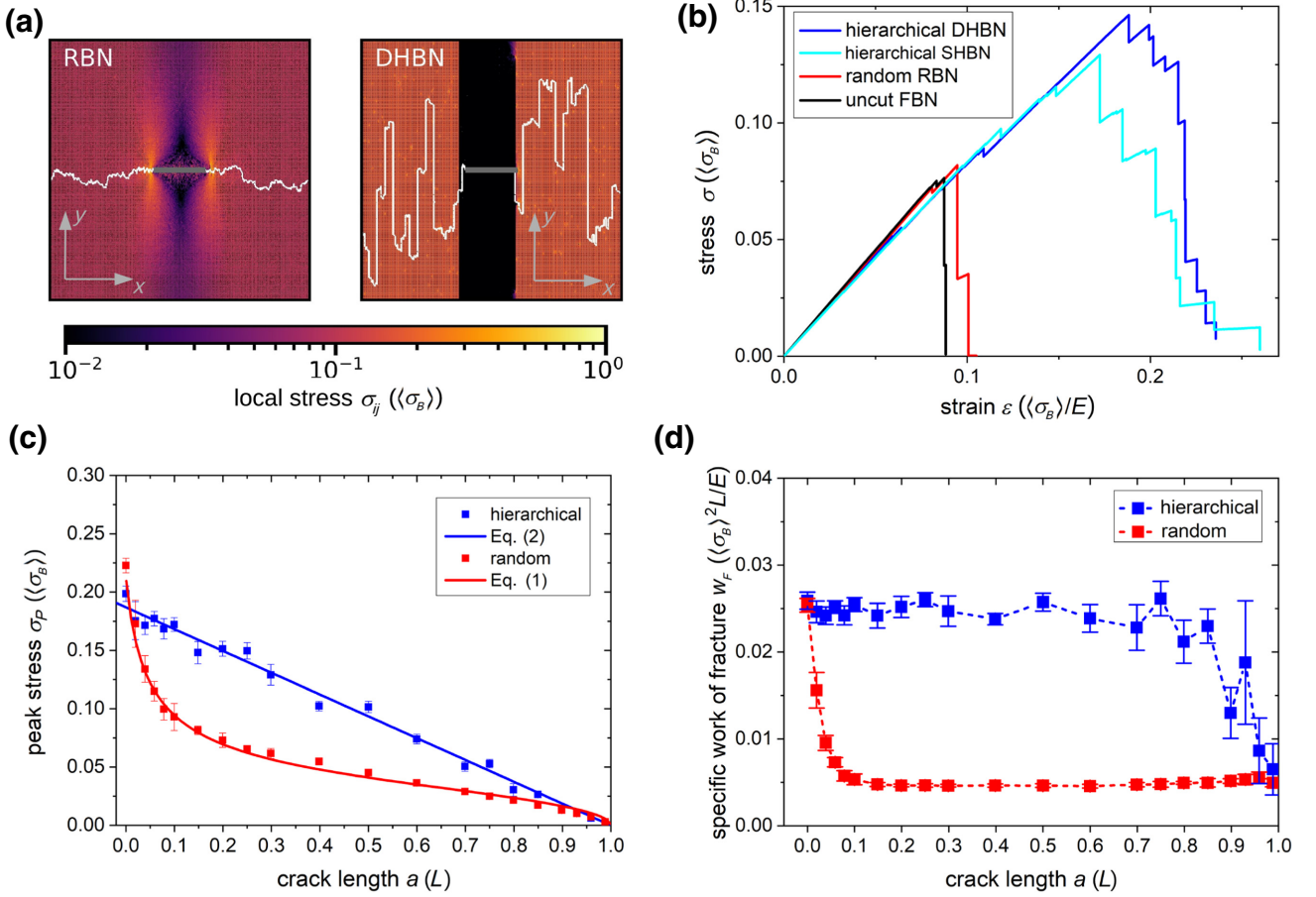


FIG. 2. Simulation results. Simulation results for hierarchical (DHBN, SHBN) and nonhierarchical (RBN, FBN) structures of size $L = 512$; (a) internal stress patterns at the peak stress, initial crack of length $a = 100$ is marked in gray, the white line indicates the fracture path, the system is loaded in tension in y direction; (b) representative stress-strain curves for different network types, crack length $a = 100$, stresses and strains are given as multiples of the mean beam failure stress $\langle\sigma_B\rangle$ (see Appendix A) and failure strain $\langle\sigma_B\rangle/E$; (c) peak stress in units of $\langle\sigma_B\rangle$ as a function of crack length for DHBN and RBN samples, all data are averaged over ten samples, the error bars indicate the corresponding standard deviation, red and blue lines represent fits according to Eqs. (1) and (2), respectively; (d) specific work of fracture for the same set of samples; the data points and error bars in (c),(d) each represent the average and standard deviation of 20 simulations.

the much higher WOF values must be attributed to diffuse damage accumulation in the bulk of the system, and hence to a strong increase of the nonessential WOF.

B. Experiments

Experiments are carried out on sheets made of paper and of polystyrene, which are endowed with gap patterns to create hierarchical subdivisions matching the DHBN and SHBN beam network morphologies. Pristine sheets and sheets with nonhierarchical gap patterns are tested for comparison. Details of specimen preparation and testing protocol are found in Appendix B.

Tensile tests on paper reveal a picture that closely matches the results obtained in the simulations (Fig. 3). This is already evident upon external inspection: hierarchical samples exhibit a super-rough crack path that

closely resembles the findings in HBN simulations [compare Fig. 2(a), right, and Fig. 3(a)]. As in the simulations, the stress-strain curves of hierarchically patterned paper sheets containing pre-existing cracks exhibit significantly enhanced peak strength σ_p and post-peak activity as compared to their nonhierarchical counterparts [Fig. 3(b)]. The dependency of failure stress on crack length again matches the simulation results: while the data for pristine and randomly patterned paper sheets follow the fracture mechanics prediction [black data points and line in Fig. 3(c)], hierarchically patterned samples exhibit a nearly linear decrease of peak strength with crack length [blue data points and line in Fig. 3(c)]. The peak strength of the hierarchically patterned samples without crack ($a = 0$) is comparable to that of randomly patterned or unpatterned samples, whereas in the presence of a crack, the hierarchically patterned samples are always stronger.

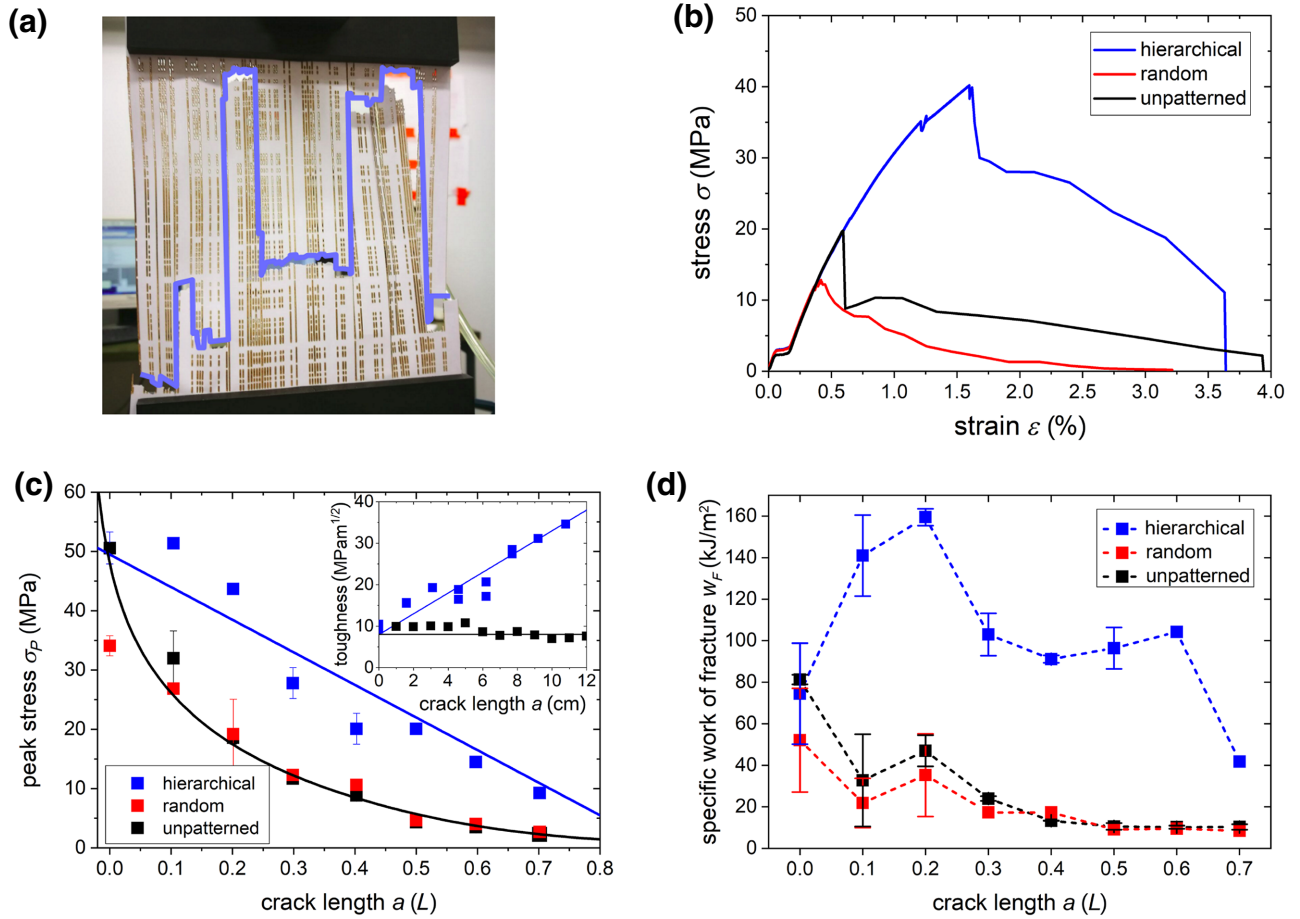


FIG. 3. Fracture experiments on paper sheets. The sample side length L corresponds to 154 mm. (a) Fractured unnotched sample with SHBN-type hierarchical cut pattern, the blue line indicates the fracture surface; (b) stress-strain curves for DHBN- and RBN-type patterned and unpatterned sheets, all with a side notch of length $a = L/5 = 31$ mm; (c) peak stress as a function of notch length for DHBN- and RBN-patterned and unpatterned sheets, black and blue lines are fits according to Eqs. (1) and (2), respectively; inset: apparent fracture toughness relating peak stress to notch length via Eq. (1); (d) specific work of fracture as a function of notch length for the same set of samples as in (c); where error bars are given, the data points represent the average of two samples while the error bars indicate the larger and smaller value.

For long cracks ($a \geq 0.5L$) the strength increase due to hierarchical patterning amounts to a factor of 4. We can use classical fracture mechanics to relate the peak strength (the stress required to induce supercritical crack propagation) to the crack length a and fracture toughness K_{Ic} via Eq. (1). Using for a plate with a side notch, the relationship $f(x) \approx (1.12 - 0.23x + 10.56x^2 - 21.74x^3 + 30.42x^4)^{-1}$ where $x = a/L$ [26], we find for unpatterned and random samples an approximately constant fracture toughness $K_{Ic} = 8.69$ MPa $m^{1/2}$. In hierarchically patterned samples, on the other hand, the factor K_{Ic} (here best denoted as apparent fracture toughness since failure does *not* proceed by propagation of the pre-existing crack) is not constant but increases with crack length [inset in Fig. 3(c)].

A significant strengthening effect by hierarchical patterning is also manifest if we consider the specific work

of fracture w_F [Fig. 3(d)]. In the limit $a \rightarrow 0$ this quantity is comparable for hierarchical and nonhierarchical samples. For nonhierarchical samples, w_F first decreases with increasing crack length and then stabilizes at a low level. In hierarchical samples, on the other hand, w_F first *increases* with crack length, shows a peak, and then stabilizes at a level that exceeds the typical WOF values of the nonhierarchical samples by a factor of about 10. We emphasize that this is not due to an increase in the work required to increase the fracture surface (essential work of fracture), as the original crack in fact does not propagate. The enhanced WOF of hierarchical samples rather represents the work expended to create damage everywhere in the sample (nonessential work of fracture), which ultimately leads to failure by damage coalescence.

For precracked nonhierarchical samples, the WOF values range between 15 and 40 kJ/m², although one cannot clearly identify a plateau value from the w_F versus a curve. These values are of the same magnitude as the values of the essential work of fracture computed from the relationship $w_{F,e} \approx K_{Ic}^2/E$. With Young's moduli $E = 4.85$ GPa for unpatterned and $E = 3.06$ GPa for randomly patterned samples, this yields values of $w_{F,e} = 15.5$ kJ/m² for unpatterned and $w_{F,e} = 24.7$ kJ/m² for randomly patterned samples. Thus, the overall picture emerging from our experiments on paper samples matches well the simulation results.

The observations on PS sheets demonstrate that hierarchically patterned SHBN-type PS samples [Fig. 4(a), right] exhibit a similar fracture surface morphology as SHBN-patterned paper sheets [Fig. 3(a)] and simulations [Fig. 2(a), right]. This morphology differs from the fracture surface of RBN-type reference samples [Fig. 4(a), left and Fig. 2(a), left]. The difference in fracture surface morphology between hierarchically patterned sheets and reference samples is associated with a significant difference in the shape of the stress-strain curves. Both unpatterned and randomly patterned sheets show almost ideally brittle macroscopic behavior. This is in stark contrast with the deformation behavior of hierarchically patterned sheets, where we see extensive post-peak activity associated with crack arrest and the nucleation and propagation of new cracks [Fig. 4(b)]. This increased post-peak activity results in a very significant enhancement of the work of fracture [Fig. 4(d)]. The dependency of peak stress on crack length in PS is well described by Eq. (1) for all types of samples [full lines in Fig. 4(c)], indicating that the peak stress is controlled by the length of the initial crack. The corresponding fit values of the fracture toughness are $K_{Ic} = 7.12$ MPam^{1/2} for random and hierarchical samples, and $K_{Ic} = 5.34$ MPam^{1/2} for unpatterned samples. We can again use these values to estimate the essential WOF, assuming brittle crack propagation. From the stress-strain curves we deduce elastic moduli $E \approx 2.8$ GPa for random and $E \approx 2$ GPa for unpatterned samples, which gives estimates of $w_{F,e} = K_{Ic}^2/E = 18$ kJ/m² for random and $w_{F,e} = K_{Ic}^2/E = 14$ kJ/m² for unpatterned samples. These values compare well with the observed WOF plateau value of around 18 kJ/m² for random and unpatterned samples [Fig. 4(d)]. We can thus conclude that the behavior of random and unpatterned samples is consistent with brittle fracture by propagation of the pre-existing crack. In hierarchical samples, on the other hand, the much higher plateau value of the WOF seen in Fig. 4(d) implies a significant nonessential work of failure.

Direct observation of the samples indicates that widespread crazing occurs away from the initial crack, which often is arrested, followed by nucleation and propagation of another crack at a different location of the sample. Thus, while the peak strength in hierarchically patterned

PS is governed by the length of the initial crack, the same is not true for the overall work of fracture, which is very significantly increased by the hierarchical patterning.

III. DISCUSSION

We demonstrate that hierarchical patterning of sheet-like materials can significantly enhance their resistance to crack propagation. Whereas samples without hierarchical patterning in all cases follow the predictions of fracture mechanics, with hierarchical patterning these predictions strongly underestimate the crack propagation resistance of the material. This effect is mainly geometrical: in our simulations as well as in the experiments on paper, the hierarchical stress redistribution introduced by an appropriate pattern of cuts offsets the effect of crack-tip stress concentrations. In our experiments on PS samples, the initial crack controls the peak strength in both hierarchically patterned samples, but the hierarchical pattern facilitates crack arrest and forces fracture to propagate in a relay-race manner by repeated nucleation, propagation, and arrest of new cracks, alongside widespread crazing.

Thus, while material-specific aspects are of relevance, the general principle of increasing fracture resilience by hierarchical patterning is demonstrated to work for quite different materials: a hypothetical material exhibiting locally perfectly elastic-brittle behavior (our simulations), a fibrous composite, which fails by fiber pull out, fiber-to-fiber bond failure, and fiber fracture (paper), and an amorphous polymer (PS), which locally fails by strain localization and crazing. We may thus conclude that “stress engineering” via the introduction of hierarchical structure provides an efficient means to increase fracture tolerance and to mitigate against the well-known fracture mechanical size effect according to which the strength of a sample is controlled by the longest crack. We note that hierarchical patterns are equally efficient in mitigating statistical size effects where strength is controlled by the weakest link in a disordered microstructure, as discussed in Appendix C and illustrated in Fig. 5. Similar notch tolerance has not been seen in kirigami materials [30,31] even when a form of hierarchical structure [32,33] has been utilized. These structures have not been able to mitigate against the propagation of a single critical crack.

The presented simulations and experiments consider situations where quasi-two-dimensional samples of simple geometry are loaded along a single axis. However, generalization is straightforward: an example demonstrating a direct three-dimensional generalization of our HBN construction is shown in Appendix D and Figs. 6(a) and 6(b) demonstrate that our general conclusions about the benefit of such hierarchical organization for improving fracture properties carry over to three-dimensional (3D) architectures. More generally speaking, the underlying principle of

dividing a load-carrying structure into load-parallel fibers and then connecting these fibers in a hierarchical manner is fairly generic and can be applied to three-dimensional structures of general geometry as well as to structures under multiaxial loading. This idea might be exploited when dealing with materials that are inherently subject to statistical scatter, as often encountered in biomaterials. The same idea might be used to mitigate against manufacturing defects as often encountered in additively manufactured (AM) materials, thus exploiting the geometrical freedom provided by AM to mitigate potential drawbacks of AM technology in view of material performance. As a caveat, we note that the effect demonstrated here is strongly anisotropic: crack propagation is efficiently suppressed only if the crack is oriented perpendicular to the hierarchically connected load-carrying fibers. For materials subject to shear loads, biaxial or even more generic loadings, more complex architectures (such as a superposition of hierarchical fabrics of different orientation) may need to be envisaged.

ACKNOWLEDGMENTS

M.Z. and S.A.H. acknowledge funding of this work by DFG through Grant No. 1Za 171-7/1, and P.M. acknowledges DFG funding under MO 3049/3-1. S.A.H. and M.P. also acknowledge participation as associate researchers in the training programme of DFG GRK 2423 FRASCAL. J.K. acknowledges funding from Academy of Finland (308235). M.J.A. acknowledges support from the European Union Horizon 2020 research and innovation programme under Grant Agreement No. 857470, from European Regional Development Fund via Foundation for Polish Science International Research Agenda PLUS programme Grant No. MAB PLUS/2018/8, and from the Academy of Finland (No. 278367 and No. 317464). T.M. acknowledges funding from The Finnish Foundation for Technology Promotion.

APPENDIX A: SIMULATION METHODS

To simulate the mechanical behavior of sheetlike materials, we rely on 2D beam network models (BNM) of (semi)brittle material behavior as used in Refs. [23,27]. We consider BNM based on a 2D simple cubic lattice of interconnected beams, which are clamped together at their intersections. The points where beams are mutually connected are referred to as nodes; a BNM of size L has $L(L+1)$ nodes. $L = 2^n$ is referred to as the network size, it is taken to be a power of 2. We measure length in units of the beam length and use a Cartesian coordinate system aligned with the [10] and [01] lattice directions. The system is assumed to be located in the domain $0 \leq x \leq L$, $0 \leq y \leq L+1$. Periodic boundary conditions are imposed in the load perpendicular (in figures, horizontal) x direction. Beams oriented parallel to the loading axis are denoted

as load-carrying (LC) beams, their number is $N_{LC} = L^2$; the LC beams form a set of L parallel fibers of length L . Beams oriented in perpendicular direction are denoted as cross-link (CL) beams, their number is N_{CL} ; a set of l horizontally connected CL beams is denoted a CL connector of length l . On the other hand, a set of l vertically adjacent CL beams that are missing or have failed is denoted as a gap of length l . A network without missing CL beams is called a full beam network.

The construction of a deterministic hierarchical beam network from a FBN can be envisaged as a hierarchical slicing operation, which starts out from a full beam network where $N_{CL} = L(L-1)$ and $N_{LC} = L^2 = 4^n$. From this starting point, a hierarchical slice pattern is obtained by removing cross links such as to create gaps, which recursively subdivide the structure into load-carrying modules of decreasing order as illustrated in Fig. 1(a): we start with a FBN of size L . This is divided by two load-parallel cuts of length $L/2 - 1$ into four lower-level modules of size $L/2$, forming two groups of two modules loaded in series; the groups are connected by a remaining, system-spanning CL connector of length L . Then, each of the four modules is again divided by two shorter cuts of length $L/4 - 1$ into four lower-level modules plus a module-spanning CL connector of length $L/2$, etc. For a structure of size $L = 2^n$, n subdivision operations are possible: n is therefore called the number of hierarchy levels. The fraction of CL beams removed in the process is $f_{CL}^* = (1/3)(1 - 2^{1-n})$, which for $n \gg 1$ converges to $f_{CL}^* = 1/3$. In experimental samples, this corresponds to a total cut length of $2^n L_S f_{CL}^*$ where L_S is the physical edge length of the sample.

A randomized version of this network structure (denoted SHBN) is obtained by randomly swapping rows and columns of the DHBN connectivity matrix, using L binary swaps of randomly chosen columns and an equal number of swaps of randomly chosen rows. An ensuing structure is illustrated in Fig. 1(b), center, for $n = 5$. Nonhierarchical reference structures are FBN and also so-called random beam networks, where the same fraction f_{CL}^* of cross-links are removed as in a (S)HBN of order n , but the locations of the removed cross-links are chosen randomly [Fig. 1(b), right].

Structures with pre-existing cracks are implemented by removing a set of a adjacent LC beams at locations $x_0 \leq x \leq x_0 + a, y = y_0$ where a is the crack length and, owing to the periodic boundary conditions in x direction, x is understood modulo L . To avoid boundary effects at the top and bottom sample edges and to ensure generic behavior, in DHBN structures the left crack endpoint (x_0, y_0) is chosen randomly within the domain $0 \leq x_0 < L, L/4 < y_0 < 3L/4$. In SHBN structures, by construction the columns and rows of the hierarchical gap pattern are randomly permuted between different realizations such that a fixed crack location can be used.

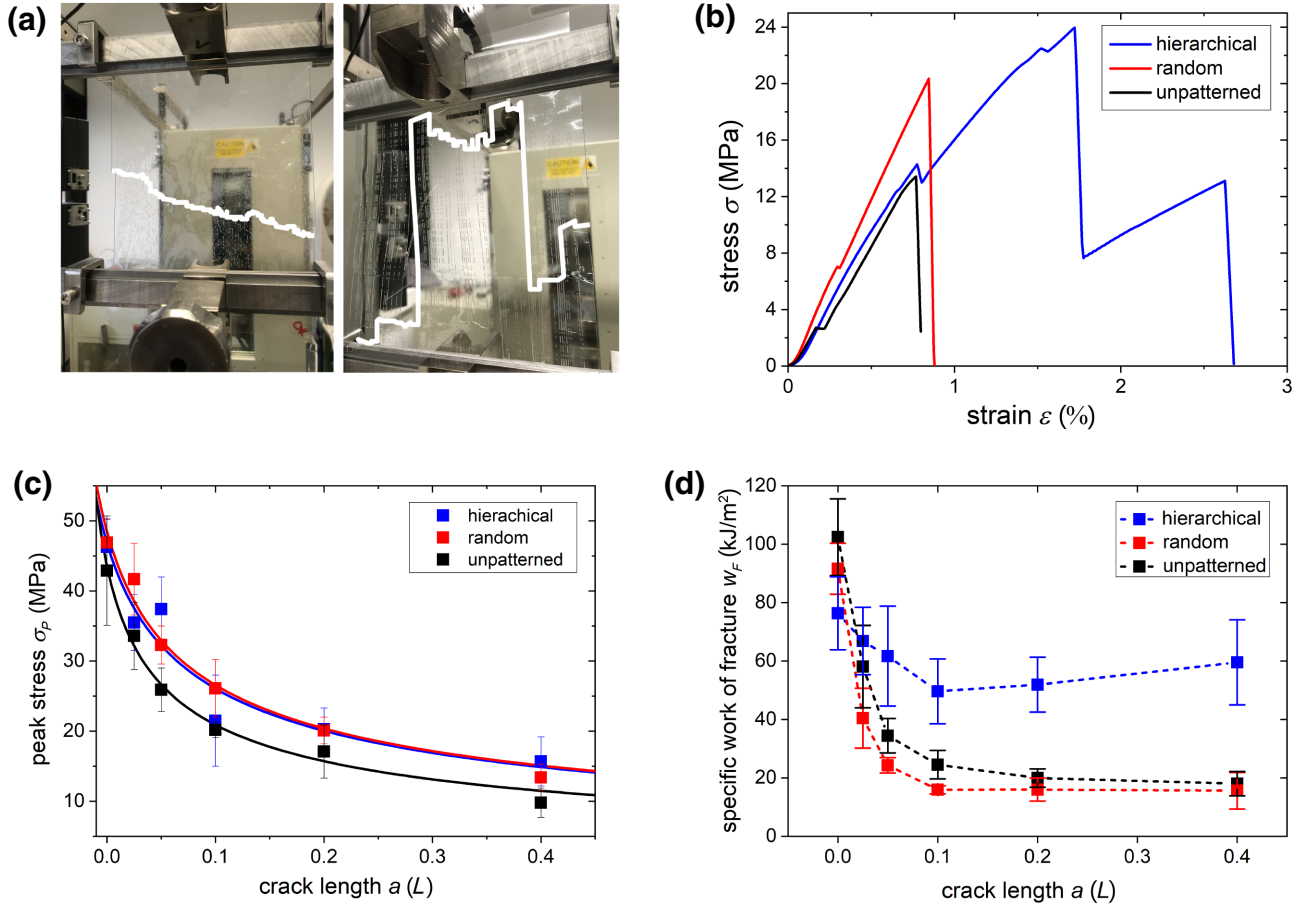


FIG. 4. Fracture experiments on PS sheets. The sample side length L corresponds to 160 mm. (a) Fractured samples with RBN cut pattern (left) and with SHBN-type cut pattern (right), initial notch length 4 mm, the fracture surfaces are traced in white; (b) stress-strain curves for sheets with SHBN patterns ($n = 7$ hierarchical levels), RBN reference patterns and unpatterned sheets, all with a side notch of length $a = 32$ mm; (c) peak stress as a function of notch length for SHBN- and RBN-patterned and unpatterned sheets, full lines are fits according to Eq. (1); (d) specific work of fracture as a function of notch length for the same set of samples as in (b); the data points and error bars in (b),(c) each represent the average and standard deviation of data from five samples.

On the beam level, we assume rigid elastic-brittle behavior, i.e., a beam behaves elastically until a stress-based failure criterion is met and then fails instantaneously and irreversibly. We measure length in units of the elementary beam length λ and assume unit beam cross section A and modulus of resistance I . In terms of nodal forces and moments the failure criterion for beam ij connecting nodes i and j then reads $\sqrt{(F_i n_i + \max[|M_i|, |M_j|]/\Lambda)^2 + 3Q_i^2} = A\sigma_{ij}$ where n_i indicates the outward normal direction of the beam end surface connecting to node i , F_i is the normal force on this surface, which can be tensile ($F_i n_i > 0$) or compressive ($F_i n_i < 0$), Q_i is the shear force, and M_i is the moment acting on this surface. The beam strength σ_{ij} is assumed to be a Weibull distributed random variable with mean value $\langle\sigma_B\rangle$, and the exponent of the Weibull distribution is denoted as β .

In the simulations, the top nodes of the network ($y = L + 1$) are displaced rigidly in y direction while the bottom

nodes ($y = 0$) are fixed. The top displacement is increased until beam stresses on one beam meet the failure criterion and the beam undergoes brittle failure. This beam is then removed and stresses are recomputed, leading to possible secondary failures as the stresses on intact beams may increase due to the load redistribution. The recomputation is continued until all remaining beams are below their failure stress. The applied displacement is then increased until another beam breaks, and the process repeats until the system is topologically disconnected.

APPENDIX B: SPECIMEN PREPARATION AND EXPERIMENTAL TESTING PROTOCOL

Experimental specimens consist of square sheets of paper and PS. They are tested in uniaxial displacement controlled tension. Pristine samples are tested alongside samples that have been sliced to create random or hierarchical cut patterns. The patterns created by a laser

cutter directly reproduce the cuts introduced, through beam removal, in the construction process of DHBN, SHBN, and RBN simulation models. In Fig. 1 these cuts, which are applied in load-parallel (vertical) direction, are shown as blue vertical lines. We test pristine paper samples without cuts, samples endowed with DHBN and SHBN patterns representing $n = 7$ hierarchical levels, and samples with RBN patterns of the same total cut length. Notches with lengths a ranging from 0 to 70% of the sheet width L are cut in load perpendicular (horizontal) direction into all samples, starting from the left edge of the sheets. For DHBN structures, notches are located randomly in the interval $L/4 \leq y \leq 3L/4$. For SHBN structures, the cuts are always located at $y = L/2$ while it is ensured that the cut patterns of different samples represent different random permutations of the DHBN connectivity matrix. In both cases, the randomization ensures that the results on notched structures are generic and not contingent on a particular location of the notch with respect to the ordered DHBN pattern.

Paper samples are produced from sheets of 75 g/m² copy paper with dimensions $154 \times 154 \times 0.1$ mm³ using a Epilog Fusion 32 laser cutter to create samples with HBN, SHBN, and RBN-like cut patterns. These samples are tested alongside pristine paper samples on a Instron ElectroPuls E1000 testing machine. Testing is carried out at room temperature with a constant imposed engineering strain rate of 2×10^{-4} s⁻¹. A sample with SHBN pattern is shown after testing in Fig. 3 (left) of the main paper, illustrating the cut pattern and showing the super-rough crack path typical of hierarchically patterned samples.

PS samples are produced from biaxially oriented, additive-free PS films of 0.05 mm thickness (Goofel-low GmbH, Hamburg, Germany). The average molecular weight is determined as 275 kg/mol with polydispersity 3.0. Sheetlike samples of dimensions $160 \times 160 \times 0.05$ mm³ are produced using a Universal VLS 2.30 laser cutter; in this case besides pristine sheets only SHBN and RBN-like patterns are considered. Testing is performed at room temperature on a Zwick Z050 tensile tester. A preload of 0.2 N is applied at a displacement rate of 20 mm/min, subsequent testing is performed at a constant speed of 50 mm/min.

APPENDIX C: HIERARCHICAL PATTERNING AND STATISTICAL SIZE EFFECTS

Fracture strength is governed by different types of size effects. In the presence of cracks, the strength of a cracked sample is often determined by the crack length as expressed by well-known relations of fracture mechanics, see Eq. (1) of the main paper. Even in the absence of cracks, the strength of disordered materials is often governed by weakest-link effects. This is most evident in long thin wires whose strength is governed by their

weakest cross section. Following standard arguments of extremal statistics, if the probability of an element to fail below stress σ is $P(\sigma)$, then the failure probability $P_N(\sigma)$ for the weakest of N elements fulfils the relation $1 - P_N(\sigma) = [1 - P(\sigma)]^N$. Specifically, if strength is Weibull distributed, $P(\sigma) = 1 - \exp[-(\sigma/\hat{\sigma})^\beta]$, then the strength of the weakest element is also Weibull distributed, $P_N(\sigma) = 1 - \exp[-(\sigma/\sigma_N)^\beta]$ where the characteristic strength of the weakest link fulfils the relation $\sigma_N = \hat{\sigma}N^{-1/\beta}$. In long thin wires of length L where cross sections of length d fail independently, we thus find a size-dependent decrease of average strength according to $\langle \sigma \rangle \propto (L/d)^{-1/\beta}$.

Because of this effect, it is unwise to mitigate against crack propagation in a sheet by slicing it parallel to the loading direction into unconnected thin ribbons forming a bundle of fibers, which are then loaded in parallel. While such a structure fulfills Eq. (2), i.e., it mitigates crack

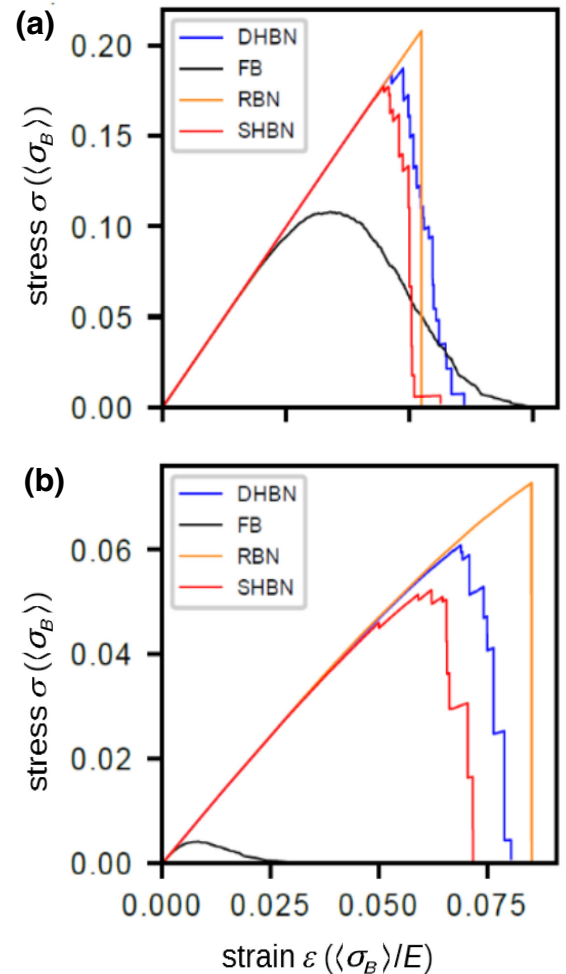


FIG. 5. Statistical size effects. Simulated stress-strain curves, $L = 1024$, the label FB refers to a bundle of 1024 unconnected fibers of length L that are loaded in parallel; top: Weibull exponent $\beta = 4$, bottom: Weibull exponent $\beta = 1.5$.

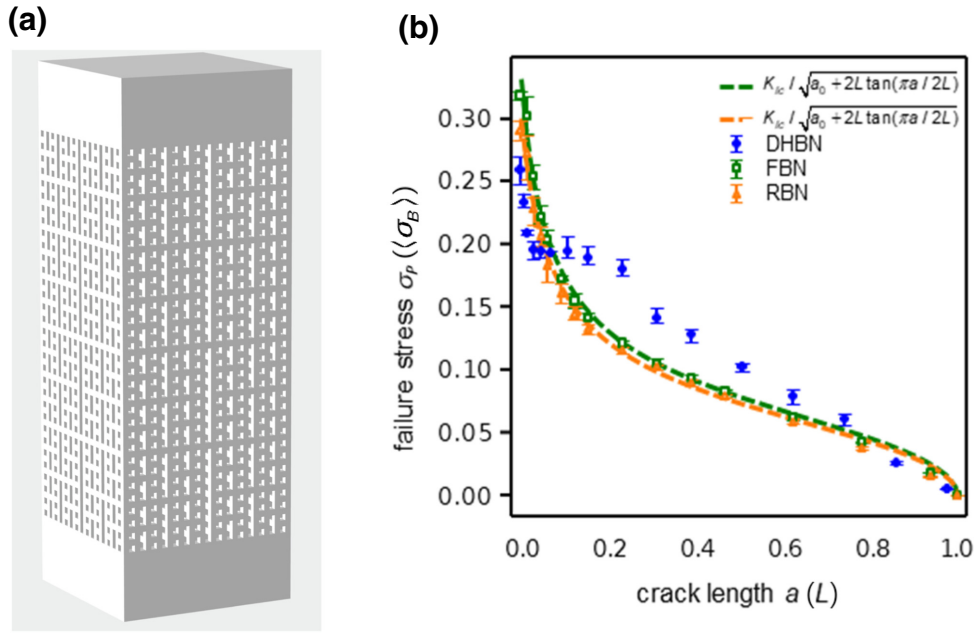


FIG. 6. Generalization to 3D. (a) Three-dimensional generalization of a 2D HBN as depicted in Fig. 1, the depicted 3D sample consists of two $n = 4$ -level hierarchical modules stacked on top of each other; (b) simulations of 3D networks of length $L = 128$ containing cracks of different lengths, peak stress versus crack length, Weibull exponent $\beta = 4$.

propagation just as efficiently as any hierarchical pattern, its performance in view of statistical size effects is much worse. First, it is known from the theory of fiber bundles that the strength of such a bundle is always less than the mean strength of the individual ribbons. Second and of note, the strength of the individual ribbons can suffer badly from statistical size effects: we can approximately envisage a ribbon of thickness d and length L as a chain of L/d patches, which are elastically weakly coupled and thus fail in a roughly independent manner. Thus, for Weibull-distributed strength of the elementary patches the overall strength of the ribbon is expected to decrease like $(L/d)^{-\beta}$. The consequences for strongly disordered materials (low β) are illustrated in Fig. 5: whereas cross-linked structures (FBN, RBN, DHBN, FHBN) are independent of the type of cross-linking about the same strength, a structure where all cross-links have been removed is very significantly weaker—an effect that becomes more pronounced as the degree of disorder and/or the system size increases.

The physical reason for this observation is simple: in a bundle of fibers, as soon as a fiber breaks at its weakest links, the remaining intact part of the fiber carries zero load. In a cross-linked structure, on the other hand, shear stress transfer between the intact parts of a broken fiber and adjacent parts of the structure ensures that these intact parts still contribute to carrying the overall load, thus making the structure inherently more resilient. It was demonstrated by Ref. [27] that this makes cross-linking necessary to achieve strength and reliability in structures composed of unreliable elements. Figure 5 indicates that this aim is achieved equally well for hierarchical and nonhierarchical cross-linking patterns. Hence, hierarchical patterning provides a means to simultaneously meet the conflicting

requirements of achieving high overall strength and high flaw tolerance (resistance to crack propagation): hierarchical patterns work just as well as fully cross-linked patterns in achieving structural redundancy that mitigates against statistical size effects, but they work as well as patterns without cross-links in mitigating against crack propagation by local stress concentrations.

APPENDIX D: GENERALIZATION TO 3D

The hierarchical construction shown in Fig. 1 can be readily generalized to 3D. On the highest level one starts with a cubic block, which is divided by four plane cuts into eight modules (two groups of four modules in parallel, separated by a “horizontal” system-spanning connecting plane). One then proceeds recursively by subdividing each of the modules. A sample consisting of two stacked hierarchical cubes, each produced via four subdivision steps, is shown in Fig. 6(a). Simulated tests of such structures alongside nonhierarchical reference structures produce a picture very similar to the 2D case discussed in the main paper, see Fig. 6(b).

- [1] R. Lakes, Materials with structural hierarchy, *Nature* **361**, 512 (1993).
- [2] N. M. Ougno, F. Bosia, and A. Carpinteri, Multiscale stochastic simulations for tensile testing of nanotube-based macroscopic cables, *Small* **4**, 1044– (2008).
- [3] P. Fratzl and R. Weinkamer, Nature’s hierarchical materials, *Prog. Mater. Sci.* **52**, 1263 (2007).
- [4] A. Gautieri, S. Vesentini, A. Redaelli, and M. J. Buehler, Hierarchical structure and nanomechanics of collagen

- microfibrils from the atomistic scale up, *Nano Lett.* **11**, 757 (2011).
- [5] J. Y. Rho, L. Kuhn-Spearing, and P. Zioupos, Mechanical properties and the hierarchical structure of bone, *Med. Eng. Phys.* **20**, 92 (1998).
 - [6] H. Gupta, J. Seto, W. Wagermaier, P. Zaslansky, P. Boesecke, and P. Fratzl, Cooperative deformation of mineral and collagen in bone at the nanoscale, *Proc. Nat. Acad. Sci.* **103**, 17741 (2006).
 - [7] D. Jiao, Z. Liu, Z. Zhang, and Z. Zhang, Intrinsic hierarchical structural imperfections in a natural ceramic of bivalve shell with distinctly graded properties, *Sci. Rep.* **5**, 12418 (2015).
 - [8] H. Gao, Application of fracture mechanics concepts to hierarchical biomechanics of bone and bone-like materials, *Int. J. Fract.* **138**, 101 (2006).
 - [9] H. Yao and H. Gao, Multi-scale cohesive laws in hierarchical materials, *Int. J. Solids Struct.* **44**, 8177 (2007).
 - [10] G. Choi, L. H. Dudte, and L. Mahadevan, Programming shape using kirigami tessellations, *Nat. Mater.* **18**, 999 (2019).
 - [11] Y. Hong, Y. Chi, S. Wu, Y. Li, Y. Zhu, and J. Yin, Boundary curvature guided programmable shape-morphing kirigami sheets, *Nat. Commun.* **13**, 1 (2022).
 - [12] A. K. Brooks, S. Chakravarty, M. Ali, and V. K. Yadavalli, Kirigami-inspired biodesign for applications in healthcare, *Adv. Mater.* **34**, 2109550 (2022).
 - [13] M. K. Blees, A. W. Barnard, P. A. Rose, S. P. Roberts, K. L. McGill, P. Y. Huang, A. R. Ruyack, J. W. Kevek, B. Kobrin, D. A. Muller, and P. L. McEuen, Graphene kirigami, *Nature* **524**, 204 (2015).
 - [14] S. Chen, Z. Liu, H. Du, C. Tang, C.-Y. Ji, B. Quan, R. Pan, L. Yang, X. Li, and C. Gu, *et al.*, Electromechanically reconfigurable optical nano-kirigami, *Nat. Commun.* **12**, 1 (2021).
 - [15] L. Xu, T. C. Shyu, and N. A. Kotov, Origami and kirigami nanocomposites, *ACS Nano* **11**, 7587 (2017).
 - [16] P. Z. Hanakata, E. D. Cubuk, D. K. Campbell, and H. S. Park, Forward and inverse design of kirigami via supervised autoencoder, *Phys. Rev. Res.* **2**, 042006 (2020).
 - [17] P. Rajak, B. Wang, K.-i. Nomura, Y. Luo, A. Nakano, R. Kalia, and P. Vashishta, Autonomous reinforcement learning agent for stretchable kirigami design of 2D materials, *npj Comput. Mater.* **7**, 1 (2021).
 - [18] M. Moshe, E. Esposito, S. Shankar, B. Bircan, I. Cohen, D. R. Nelson, and M. J. Bowick, Kirigami Mechanics as Stress Relief by Elastic Charges, *Phys. Rev. Lett.* **122**, 048001 (2019).
 - [19] Y. Bar-Sinai, G. Librandi, K. Bertoldi, and M. Moshe, Geometric charges and nonlinear elasticity of two-dimensional elastic metamaterials, *Proc. Nat. Acad. Sci.* **117**, 10195 (2020).
 - [20] M. Czajkowski, C. Coulais, M. van Hecke, and D. Rocklin, Conformal elasticity of mechanism-based metamaterials, *Nat. Commun.* **13**, 1 (2022).
 - [21] M. J. Alava, P. K. V. V. Nukala, and S. Zapperi, Statistical models of fracture, *Adv. Phys.* **55**, 349 (2006).
 - [22] P. Moretti, B. Dietemann, N. Esfandiary, and M. Zaiser, Avalanche precursors of failure in hierarchical fuse networks, *Sci. Rep.* **8**, 1 (2018).
 - [23] S. A. Hosseini, P. Moretti, D. Konstantinidis, and M. Zaiser, Beam network model for fracture of materials with hierarchical microstructure, *Int. J. Fract.* **227**, 243 (2021).
 - [24] See Movie S1 at <http://link.aps.org/supplemental/10.1103/PhysRevApplied.18.044035> for a typical simulation.
 - [25] M. J. Alava, P. K. Nukala, and S. Zapperi, Role of Disorder in the Size Scaling of Material Strength, *Phys. Rev. Lett.* **100**, 055502 (2008).
 - [26] H. Tada, P. C. Paris, and G. R. Irwin, *The Stress Analysis of Cracks Handbook* (The American Society of Mechanical Engineers, New York, 2000).
 - [27] S. A. Hosseini, P. Moretti, and M. Zaiser, A beam network model approach to strength optimization of disordered fibrous materials, *Adv. Eng. Mater.* **22**, 1901013 (2020).
 - [28] A. Martinez, J. Gamez-Perez, M. Sanchez-Soto, J. I. Velasco, O. Santana, and M. L. Maspocho, The essential work of fracture (EWF) method—analyzing the post-yielding fracture mechanics of polymers, *Eng. Fail. Anal.* **16**, 2604 (2009).
 - [29] Y.-W. Mai and P. Powell, Essential work of fracture and J-integral measurements for ductile polymers, *J. Polym. Sci. Part B: Polym. Phys.* **29**, 785 (1991).
 - [30] T. C. Shyu, P. F. Damasceno, P. M. Dodd, A. Lamoureux, L. Xu, M. Shlian, M. Shtein, S. C. Glotzer, and N. A. Kotov, A kirigami approach to engineering elasticity in nanocomposites through patterned defects, *Nat. Mater.* **14**, 785 (2015).
 - [31] B. Zheng and G. X. Gu, Tuning the graphene mechanical anisotropy via defect engineering, *Carbon* **155**, 697 (2019).
 - [32] Y. Tang, G. Lin, L. Han, S. Qiu, S. Yang, and J. Yin, Design of hierarchically cut hinges for highly stretchable and reconfigurable metamaterials with enhanced strength, *Adv. Mater.* **27**, 7181 (2015).
 - [33] N. An, A. G. Domel, J. Zhou, A. Rafsanjani, and K. Bertoldi, Programmable hierarchical kirigami, *Adv. Funct. Mater.* **30**, 1906711 (2020).